Thermodynamic feasible photoelectron transfer from bioactive π-expanded imidazole luminophore to ZnO nanocrystal

Journal:	*New Journal of Chemistry*
Manuscript ID:	NJ-ART-11-2014-002003.R1
Article Type:	Paper
Date Submitted by the Author:	11-Dec-2014
Complete List of Authors:	Jayabharathi, Jayaraman; Annamalai University, Chemistry Karunakaran, C. ; Annamalai University, Chemistry Kalaiarasi, Vellaikannu; Annamalai university, chemistry
Note: The following files were submitted by the author for peer review, but cannot be converted to PDF. You must view these files (e.g. movies) online.	
Figures.zip	

Table of contents (TOC)

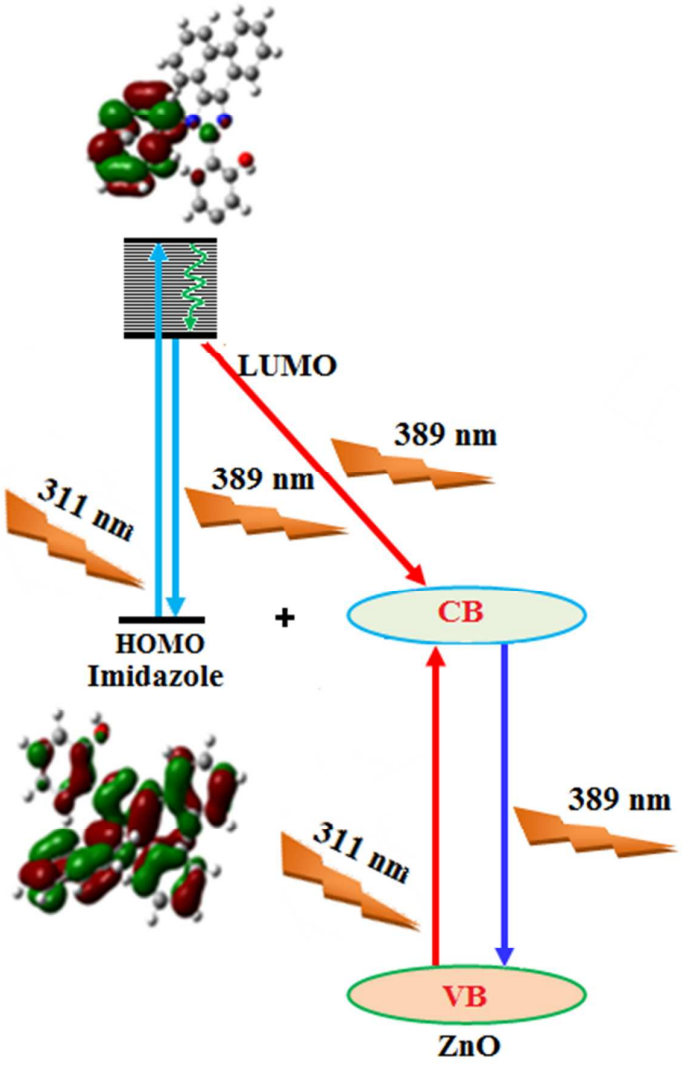

Chemical affinity between the nitrogen atom of the imidazole and zinc ion on the surface of the nano oxide may be a reason for strong interaction of the ligand on nanoparticle causes the enhancement.

Thermodynamic feasible photoelectron transfer from bioactive π-expanded imidazole luminophore to ZnO nanocrystals

Jayaraman Jayabharathi*, Chockalingam Karunakaran, Vellaikannu Kalaiarasi

Department of Chemistry, Annamalai University, Annamalainagar 608 002, Tamilnadu, India.

* Address for correspondence

Dr. J. Jayabharathi
Professor of Chemistry
Department of Chemistry
Annamalai University
Annamalainagar 608 002
Tamilnadu, India.
Tel: +91 9443940735
E-mail: jtchalam2005@yahoo.co.in

* Corresponding author. Tel.: +91 9443940735
E-mail address: jtchalam2005@yahoo.co.in

Thermodynamic feasible photoelectron transfer from bioactive π-expanded imidazole luminophore to ZnO nanocrystals

Jayaraman Jayabharathi*, Chockalingam Karunakaran, Vellaikannu Kalaiarasi

Department of Chemistry, Annamalai University, Annamalainagar 608 002, Tamilnadu, India.

Abstract

The photoinduced electron transfer (PET) based sensor, 2-(1-(naphthalene-1-yl)-4,5-diphenyl-1H-imidazol-2-yl)phenol was synthesised and characterized by spectral techniques. Absorption, emission, lifetime and cyclic voltammetric studies have been made to probe the binding interaction between imidazole and ZnO nanocrystals. The nanocrystalline ZnO enhances the absorbance and emission intensity of imidazole and the binding constant for the formation of imidazole -ZnO composite has been obtained. The band gap energy of ZnO is greater than the excited state energy of imidazole and the emission enhancement is only due to electron transfer process. TEM, SEM and EDX spectra confirmed the binding of imidazole with nanocrystalline ZnO. Theoretical investigation reveals that small Zn_nO_n clusters ($n < 9$) and their imidazole-ZnO composites are stabilized in 2D ring geometries whereas the larger cluster $Zn_{10}O_{10}$ and its imidazole-ZnO composite prefers 3D cage structures. The ring to cage crossover of ZnO clusters is studied by analyzing the Zn-$\widehat{O}$-Zn and O-$\widehat{Zn}$-O bond angles, Zn-O bond length and number of bonds. Binding energy, energy gap, binding site and adsorption strength of imidazole with different ZnO clusters show that $Zn^{2+}$of ZnO clusters prefers to bind with the azomethine nitrogen atom (N-site) relative to other binding site (O-site). The synthesized imidazole is an efficient fluorescent chemosensor for Zn^{2+} ion; it binds with Zn^{2+} ion in aqueous alcohol strongly to exhibit the sensing behaviour.

Keywords: Imidazole; PET; ZnO nanocrystal; Imidazole -ZnO composite; Chemosensor; DFT.

* Corresponding author. Tel.: +91 9443940735
E-mail address: jtchalam2005@yahoo.co.in

1. Introduction

The II–VI semiconductor nanocrystals are known for their photostability, high photoluminescence quantum yield, broad absorption with high molar extinction coefficient and their symmetric, narrow and tunable emission spanning from UV to near IR. These properties make them attractive for numerous applications, ranging from light-emitting diodes to bioimaging, biolabeling and sensing with performances that are significantly superior to their organic counterparts [1,2]. Although many smart fluorescent organic dyes have been intensively investigated for sensing a variety of target molecules, because of photoinduced electron transfer (PET) and energy transfer [3], construction of II–VI semiconductor based nanohybrids for recognition and sensing gains importance in applications of nanomaterials [3]. ZnO nanoparticles have unique physical and chemical properties and potential biomedical applications by virtue of their nontoxic nature, low cost, biosafety, biocompatibility and wide usage in daily life such as drug carriers, cosmetics, etc., [4-10]. ZnO nanoparticles can kill cancer and activated human T cells, suggesting biotherapeutic functionality of this novel material [11].The photoactive surfaces of the nanoparticles produce reactive oxygen species that can potentially cause oxidative stress which leads to cellular protein, lipid and DNA damage [12-14]. DFT calculation on ZnO clusters is widely analysed [15] and binding interaction of nano metal oxides with biological molecules viz., adenine, guanine, cytosine, thymine, etc., is of current interest in biomedical nanotechnology [16-20]. Nano ZnO prefers to bind with a ring nitrogen atom (N-site) relative to other binding sites of the DNA bases; the adsorption strength of ZnO with the N-site of guanine is much higher than other sites [21]. In order to analyse the properties of materials at the nano level a detailed study of nano metal oxide–bioactive molecule interaction is required. Joshi *et al*., [22] studied the interaction of nanoclusters with tryptophan and the results show that the binding of −COOH group (C-site) with ZnO clusters is energetically

more favourable than the other interacting sites such as indole and amine groups in tryptophan. The development of fluorescent sensors for zinc [23], magnesium [24] and alkali metal cations [25] and anions such as halides [26] and carboxylates [27] is of enormous interest for medical diagnostics. Photoinduced energy transfer (PET) mechanism is an elegant, sensitive and effective way to identify the presence of protons [28], metal ions [29], anions [30] and neutral molecules [31]. The PET chemosensor contains a luminescent species with a recognition group has been analysed [32]. In the unbound fluorophore, the electron transfer between the lone pair of the recognition group and the relevant orbitals of the luminophore results quenching whereas upon binding, the lone pair of the recognition group involved in bond formation results enhancement of fluorescence. In continuation our research [33], in this article we report the binding interaction between newly synthesised imidazole with pristine ZnO. The observed enhancement of emission is ascribed to photoelectron (PET) transfer process. For the first time, the binding of bioactive imidazole with ZnO clusters has been analysed in terms of their size, binding energy, geometry, binding site, bond length and HOMO–LUMO energies. The experimental and theoretical results confirm the formation of ≥N–Zn bond in imidazole–ZnO composites. There is an overlap occurring between the d-orbital of zinc and azomethine nitrogen atoms which lead to a greater binding energy for N site. PET mechanism for imidazole-Zn^{2+} complex has also been discussed.

2. Materials and spectral measurements

Benzil, 2-hydroxybenzaldehyde, α-naphthylamine and all other reagents used were of analytical grade. The pristine ZnO used was that supplied by Sigma-Aldrich [34]. The ^{1}H NMR and proton decoupled^{13}C NMR spectra were recorded at room temperature using a Bruker 400 MHz NMR spectrometer operating at 400 and 100 MHz, respectively. The mass spectra of the samples were obtained using a Thermo Fischer LC-Mass spectrometer in FAB mode. The UV-vis absorption and emission spectra were recorded with a PerkinElmer

Lambda 35 spectrophotometer and a PerkinElmer LS55 spectrofluorimeter, respectively. Lifetime measurements were carried out with a nanosecond time correlated single photon counting (TCSPC) spectrometer. The decay was analyzed using DAS6 software. The cyclic voltammetric analysis was performed with a CHI 630A potentiostat-electrochemical analyzer at a scan rate of 100 mV s^{-1} using 0.1 M tetra(n-butyl)-ammonium hexafluorophosphate as supporting electrolyte with Ag/Ag^{+} (0.01 M $AgNO_3$) as the reference electrode and Pt electrode as the working electrode under nitrogen atmosphere at room temperature. The energies of the highest occupied molecular orbital (HOMO) and lowest unoccupied molecular orbital (LUMO) [33] were calculated using the following equations, $E_{HOMO} = 4.4 + E_{(onset)}$; $E_{LUMO} = E_{HOMO} - 1239/\lambda_{abs}$. The powder X-ray diffractogram (XRD) was recorded with a PAN analytical X'Pert PRO diffractometer using Cu K_α rays at 1.5406 A^0 with a tube current of 30 mA at 40 kV. A JEOL JSM 10LV scanning electron microscope (SEM) equipped with a highly sensitive back scattered detector and low vacuum secondary detector was used to get the SEM image of the sample. The UV-vis diffuse reflectance spectra (DRS) were recorded with a PerkinElmer Lambda 35 spectrophotometer with RSA-PE-20 integrating sphere. The quantum chemical calculations were performed using the Gaussian 03 [35] package.

2.1. Synthesis of 2-(1-(naphthalene-1-yl)-4,5-diphenyl-1H-imidazol-2-yl)phenol[NDIP]

A mixture of 2-hydroxybenzaldehyde (1 mmol), benzil (1 mmol), α-napthylamine (1 mmol), ammonium acetate (1mmol) and InF_3 (1 mol %) was stirred at 80 °C for 2h. The crude imidazole was purified by column chromatography using benzene: ethyl acetate (9:1) as the eluent. M.p. 248 ºC., ^{1}H NMR (400 MHz, $CDCl_3$): δ, 11.98 (s, 1H) 7.27 (d, J = 9.6 Hz, 3H), 7.32 (d, J = 8.8 Hz, 6H), 7.37 (t, 3H), 7.44-7.94 (m, 10H),. ^{13}C NMR (100 MHz, $CDCl_3$ and DMSO):δ 125.38, 127.62, 127.86, 128.66, 128.90, 129.05, 129.52, 132.63, 145.87. MS: m/z. 438 [M^+].

2.1.1Synthesis of imidazole-ZnO composite

About 1mmol of imidazole in dimethyl sulphoxide (1mL) was added to 1mmol of ZnO nanoparticles suspended in dimethyl sulphoxide (1mL) under constant stirring for 3 h. The solid was filtered, washed with dimethyl sulphoxide and dried at 110 ºC.

2.1.2. Synthesis of complex imidazole- Zn^{2+} ion

A mixture of imidazole (1 mmol) and $Zn(CH_3COO)_2 \cdot 4H_2O$ (0.5 mmol) in ethanol (20 mL) was stirred for three days at room temperature and the formed crystals were filtered. Anal. calcd. for $C_{31}H_{21}N_2OZn$: C, 74.04; H, 4.21; N, 5.57. Found: C, 73.96; H, 4.01; N, 5.03. ^{1}H NMR (400 MHz, DMSO): δ, 7.31 (d, J = 9.3Hz, 3H), 7.28 (d, J = 8.3Hz, 6H), 7.32 (t, J = 8.1Hz, 3H), 7.36-7.95 (m, 10H),. ^{13}C NMR (100 MHz, $CDCl_3$ and DMSO):δ 125.42, 127.57, 127.83, 128.69, 128.94, 129.12, 129.61, 132.67, 145.85. MS: m/z. 501 [M^+]. IR (cm^{-1}): 945.10 (Zn–O), 469.51 (Zn–N).

3. Results and discussion

3.1. Morphology and band gap of imidazole-ZnO composite

Pristine ZnO is of wurtzite structure with average crystallite size (*D*) and surface area (*S*) as 32 nm and 33 $m^2 g^{-1}$, respectively [26]. Figure 1 displays the X-ray diffraction pattern (XRD) of imidazole- ZnO composite. The diffraction pattern matches with the JCPDS pattern of zincite (89-7102) and the crystal structure of imidazole-ZnO composite is primitive hexagonal with crystal constants *a* and *b* as 3.249A$^\circ$ and *c* as 5.025 A$^\circ$, respectively. The average crystallite size (L) of imidazole-ZnO composite has been deduced as 25 nm which has been obtained from the full width at half maximum (FWHM, β) of the most intense peak using the Scherrer equation, $L = 0.9\ \lambda / \beta \cos\theta$, where λ is the wavelength of the X-rays used and θ is the diffraction angle. The specific surface area (*S*) of the imidazole-ZnO composite has been obtained using the relationship, $S = 6/\rho L$, where *L* is the average particle size and ρ

is the material density. The results are in accordance with the crystal size and the calculated surface area is 61.3 $m^2 g^{-1}$.

The SEM and EDX spectra of imidazole-ZnO composite and pristine ZnO nanocrystals are shown in Figures 1 and 2, respectively. The SEM images show that binding interaction of imidazole significantly modifies the morphology of ZnO nanocrystals and confirm the binding of imidazole on ZnO nanocrystalline surface. The absence of signals other than zinc, oxygen, carbon and nitrogen confirms the purity of the synthesized imidazole-ZnO composite. The TEM image at high resolution is displayed as inset in Figure 2 which shows the lattice fringes of the nanocrystals. The observed *d*-spacing corresponds to the 100-plane of hexagonal ZnO. The diffused reflectance spectra of the samples are displayed in Figure 3.The reflectance is presented in terms of the Kubelka-Munk (KM) function. The DRS show the band gaps as 3.20 and 3.22 eV. The observed band gaps are in agreement with the mean crystallite sizes of the ZnO nanoparticles and imidazole-ZnO composite. The decrease in the average crystallite size from 32 to15.1 nm has resulted in the increase of band gap energy from 3.20 to 3.22 eV.

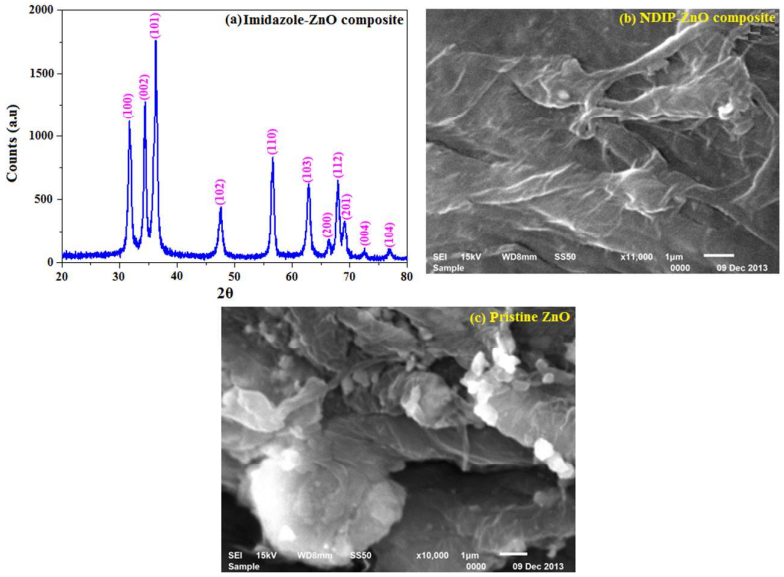

Figure 1. (**a**) X-ray diffraction pattern (XRD) of imidazole-ZnO composite; SEM images of (**b**) imidazole-ZnO composite; (**c**) pristine ZnO

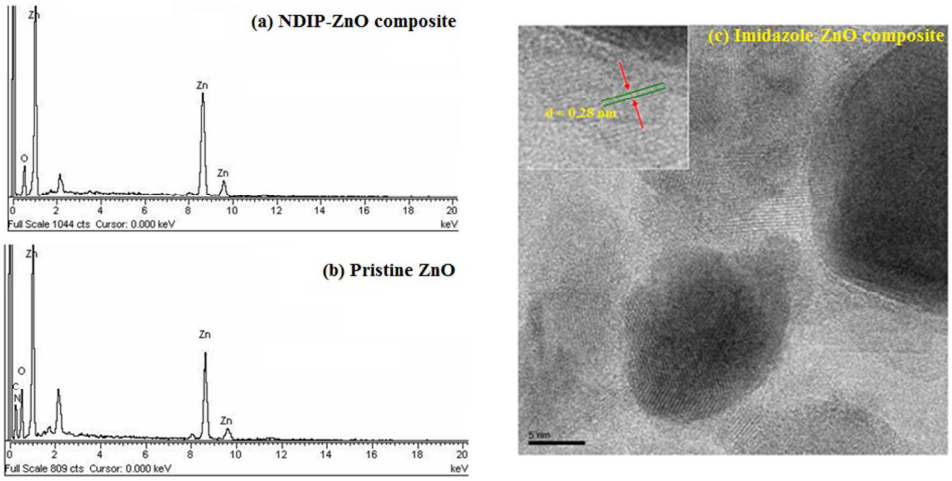

Figure 2. EDX spectra of (**a**) imidazole-ZnO composite; (**b**) pristine ZnO; (**c**) TEM image of (**a**) imidazole-ZnO composite

3.2. Photoelectron transfer

The absorption and emission spectra of imidazole in the presence and absence of ZnO nanoparticles dispersed at different loading were recorded and shown in Figure 3. The nanoparticles enhance the absorbance and emission intensity of imidazole without shifting its absorption maximum at 311 nm and emission maximum at 389 nm. The enhanced absorbance and emission intensity observed with the dispersed semiconductor nanoparticles is due to the formation of the imidazole-ZnO composite and the binding constant (*K*) has been calculated as $2.48 \times 10^7\ M^{-1}$. Such a large binding constant indicates that imidazole is strongly associated to the surface of nanocrystals by electrostatic interactions. The obtained large binding constant is because of the surface area; the surface area of the former is smaller than that of the latter. The greater interaction of smaller nanocrystals with imidazole is not only due to the large surface area of the smaller nanocrystals but also because of larger surface curvature of the smaller nanocrystals. The larger surface curvature reduces the steric hindrance between the surface binding molecules and provides a large number of unsaturated dangling bonds on the nanocrystal surface and enhances the binding interaction.

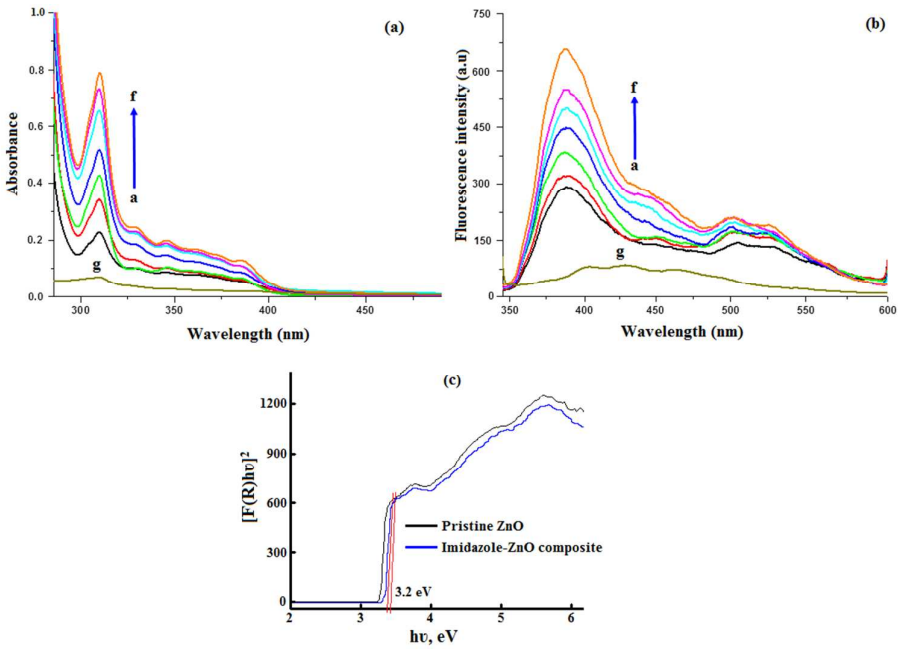

Figure 3. (**a**) Absorption spectra of (a) 10 μM imidazole, (b→f) 10 μM imidazole with ZnO nanoparticles (20→100 nM) and (g) ZnO nanoparticles (100 μM); (**b**) Emission spectra of (a) 10 μM imidazole, (b → f) 10 nM imidazole with ZnO nanoparticles 2→10 nM) and (g) ZnO nanoparticles (10 nM); (**c**) DRS of imidazole-ZnO composite and pristine ZnO; (**c**) Diffused reflectance spectra of pristine ZnO and imidazole-ZnO composite

The fluorescence enhancement may be attributed to electron transfer or energy transfer process. As shown in Figure 4, the band gap energy of ZnO is greater than the excited state energy of imidazole and there is no overlap between the emission spectrum of imidazole with the absorption spectrum of ZnO nanoparticles. The above inference excluded the possibility of energy transfer from imidazole to ZnO nanoparticles. From the onset oxidation potential (E_{ox}) and the onset reduction potential (E_{red}) of the imidazole derivative, HOMO and LUMO energies were calculated according to the following equations, HOMO = −e(E_{ox} + 4.71) (eV); LUMO = −e(E_{red} + 4.71) (eV). On the basis of the HOMO and LUMO energy levels of imidazole and CB energy level of ZnO (Figure 4), the electron injection is thermodynamically allowed from the excited singlet of the imidazole to the CB of ZnO. Figure 4 presents the HOMO and LUMO energy levels of an isolated imidazole molecule

along with the CB and valence band (VB) edges of nanocrystalline ZnO. On adsorption of the imidazole on ZnO surface, the HOMO and LUMO may interact with CB and VB of pristine ZnO and as a consequence the energy levels of HOMO and LUMO may be lowered.

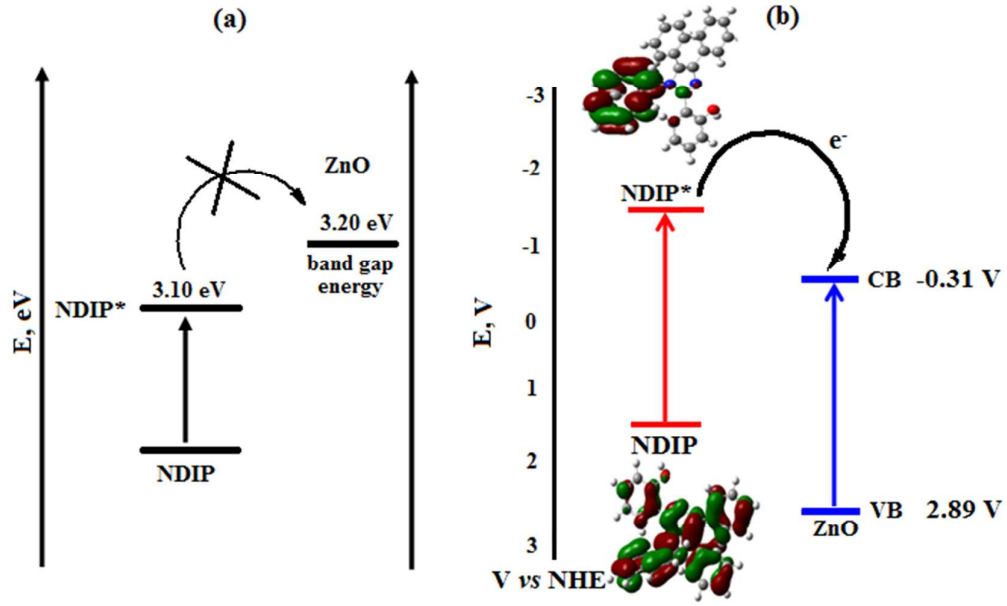

Figure 4. (**a**) Energy level diagram of imidazole and ZnO; (**b**) Energy level diagram describing the conduction and valence bands of ZnO and the electron donating energy level of imidazole

The modified HOMO and LUMO energy levels presented in Figure 5 suggest enhancement of fluorescence of imidazole by ZnO nanocrystal. On illumination at 311nm both the imidazole and pristine ZnO are excited. Dual emission is expected due to LUMO → HOMO and CB → VB electron transfer and the excited imidazole emits fluorescence at 389 nm. Also possible is electron jump from the excited imidazole to the nanocrystals. The electron in the LUMO of the excited imidazole is of higher energy compared to that of the CB of ZnO nanocrystals. The emission intensity of imidazole bound to ZnO is far larger than that of the isolated molecule. In addition, emission from the LUMO of the imidazole adsorbed on ZnO to the CB of ZnO at 389 nm is possible. Due to the additional path opened up for emission, the emission intensity is increased. On interaction of imidazole with pristine ZnO, the polar ZnO surface enhances the delocalisation of the π

electrons and lowers the HOMO and LUMO energy levels of the adsorbed imidazole due to imidazole–ZnO composite formation [36]. Therefore, the additional path opened due to LUMO → CB electron jump increases the intensity of emission at 389 nm (Figure 5). The chemical affinity between the nitrogen atom of the imidazole and zinc ion on the surface of the nano zinc oxide may be a reason for the strong interaction of the ligand with nanoparticles causing the enhancement.

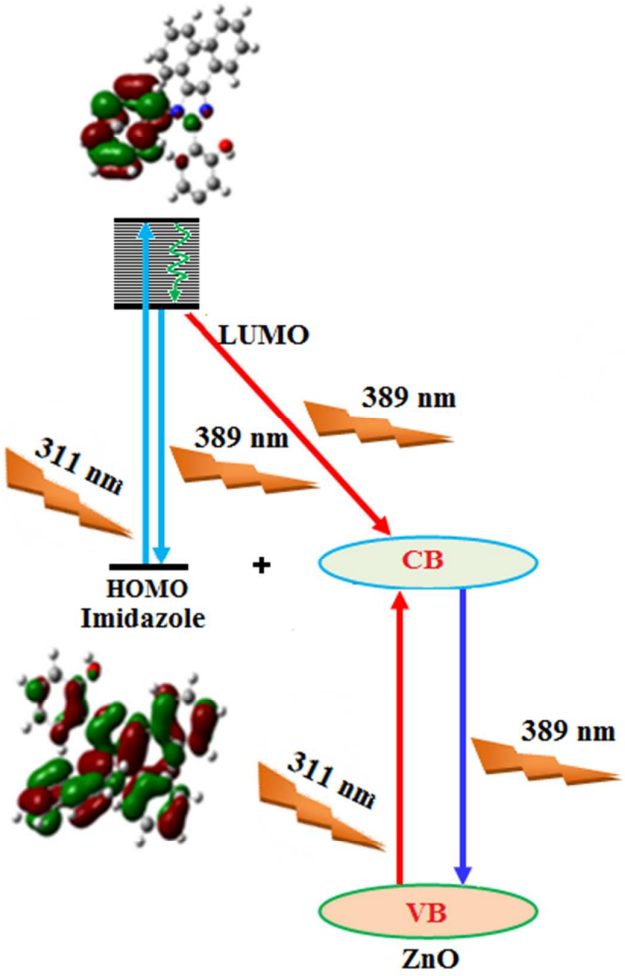

Figure 5. Enhancement of fluorescence of imidazole by ZnO nanocrystals

The thermodynamic feasibility of excited state electron transfer reaction has been confirmed by employing Rehm-Weller expression [36], $\Delta G_{et} = E^{1/2}{}_{(ox)} - E^{1/2}{}_{(red)} - E_s + C$, where $E^{1/2}{}_{ox}$ is the oxidation potential of imidazole, $E^{1/2}{}_{red}$ is the reduction potential of ZnO

nanoparticles, i.e., the conduction band potential of nanoparticle, E_s is the excited state energy of imidazole and C is the coulombic term. Since the imidazole is neutral and the solvent used is polar in nature, the coulombic term in the above expression can be neglected. The negative ΔG_{et} calculated as −0.33 eV indicates the thermodynamic feasibility of the electron transfer process [37].

3.3. Decay lifetime

Time-resolved fluorescence experiments using time correlated single photon counting (TCSPC) technique were carried out to analyze the electron transfer process from excited imidazole to nanocrystals. The experimental data were fitted to a biexponentials decay, $f(t) = \alpha_1 \exp(-t/\tau_1) + \alpha_2 \exp(-t/\tau_2)$ where α_1 and τ_1 are respectively, the pre-exponential factor and lifetime of the various excited states involved. Figure 6 displays the bi exponential decay of imidazole revealing that imidazole is in two excited states - one is likely to be the configuration in which the aryl is perpendicular with the imidazole ring [excited state I] and the other is the one in which the same is coplanar with the imidazole ring [excited state II]. The X-ray crystal structure [38] and theoretical calculation [35] show the perpendicular configuration as the most stable one and hence the observed longer lifetime is attributed to the same. The observed biexponential decay indicates that the imidazole-ZnO composite formation is possible with both the conformation of imidazole. The perpendicular conformation of imidazole binds with the nanoparticles is predominant than the other one with the planar conformation. The fluorescence decay curves of all nanoparticles with imidazole were recorded in ethanol. Laser excitation was set at 260 nm and the fluorescence signal was measured at emission wavelength of individual compound.

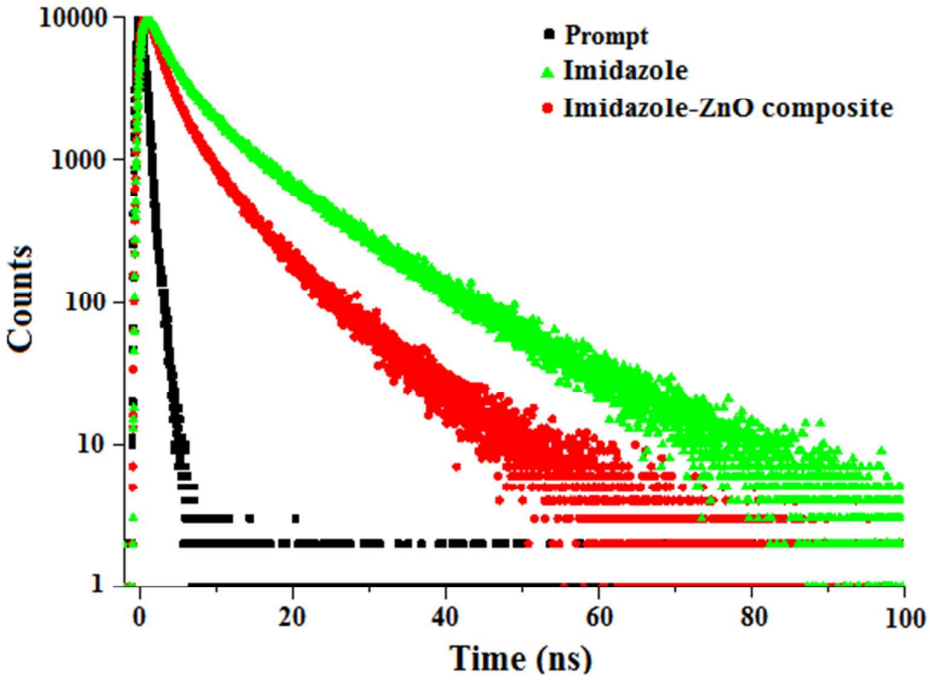

Figure 6. Fluorescence lifetime spectra of imidazole and imidazole - ZnO composite

The radiative (k_r) and non-radiative (k_{nr}) decay of the excited state have been obtained using the quantum yield (Φ) and lifetime (τ). The formula employed to calculate the k_r and k_{nr} are, $k_r = \Phi / \tau$; $k_{nr} = (1/\tau) - (\Phi / \tau)$ and $\tau = (k_r + k_{nr})^{-1}$. The decay time of imidazole - ZnO composite and imidazole are 3.23 and 5.13 ns, respectively and the radiative rate constant (k_r) of imidazole - ZnO composite and imidazole are 12.7×10^7 s^{-1} and 8.0×10^7 s^{-1}, respectively. The non-radiative rate constant (k_{nr}) of imidazole-ZnO composite and imidazole are 18.4×10^7 s^{-1} and 11.5×10^7 s^{-1}, respectively. ZnO nanocrystals bound to imidazole modifies the fluorescence lifetime. The decay times of imidazole-ZnO composite are distinctly shorter than the imidazole. This is again in line with the occurrence of electron transfer from imidazole to the nanocrystals. The rate constant for the electron transfer (k_{et}) can be calculated by using the equation, $k_{et}=1/\tau_{ads}- 1/\tau$ and the calculated value of k_{et} is 1.1×10^8 s^{-1}. The observed lifetime is also indicative of the fact that the imidazole interaction with ZnO nanocrystals results in electron transfer.

3.4 Evidence for imidazole-ZnO composite formation

Cyclic voltammetric studies were carried out to probe the efficient binding of ZnO nanoparticles with imidazole. Figure 7 shows the cyclic voltammogram (CV) of imidazole, and imidazole-ZnO composite. The composite shows a shift in peak potentials along with decrease in peak current [39]. It is evident that the ZnO nanoparticles have efficient binding with imidazole which supports the electronic spectral results. The FT-IR spectra of prisitine ZnO, imidazole and imidazole-ZnO composite are displayed in Figure 8. In the case of bare ZnO sample, Zn-O stretching vibration is observed at 445 cm^{-1}. For imidazole-ZnO composite, C=C and C-O-C stretching vibrations are observed around 1512 and 1339 cm^{-1} in addition to the Zn-O stretching mode at 460 cm^{-1}. The frequency observed around 1612 cm^{-1} by imidazole and imidazole -ZnO composite corresponds to C=N function. The absorption around 3059 cm^{-1} is due to ≥C-H of imidazole and imidazole -ZnO composite. The peak at ~ 952 cm^{-1} is likely due to the phenyl C-H stretching.

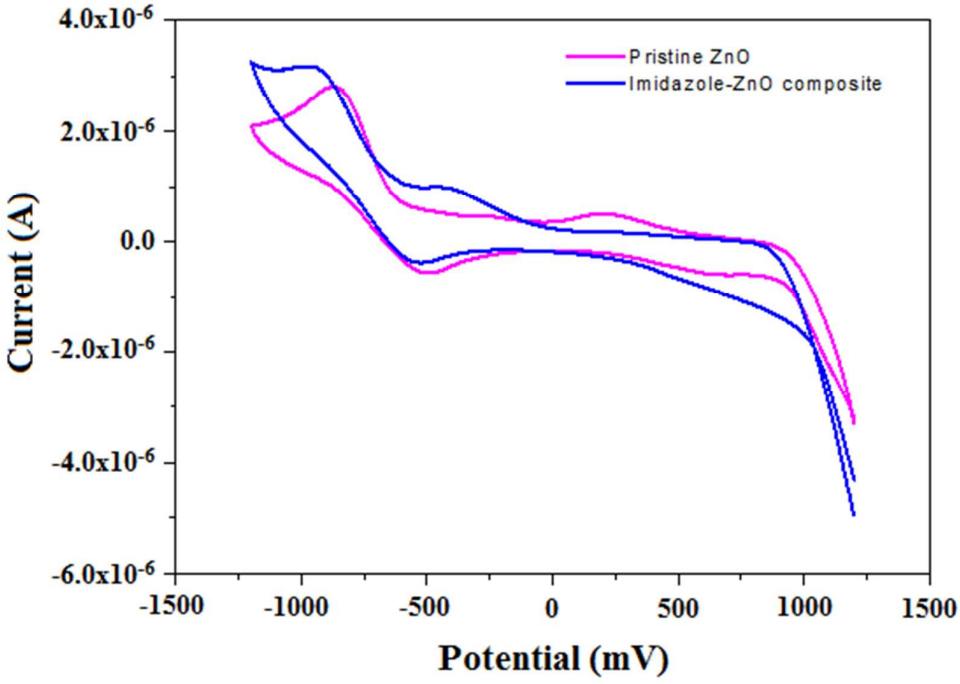

Figure 7. Cyclic voltammogram of imidazole along with imidazole–ZnO composite

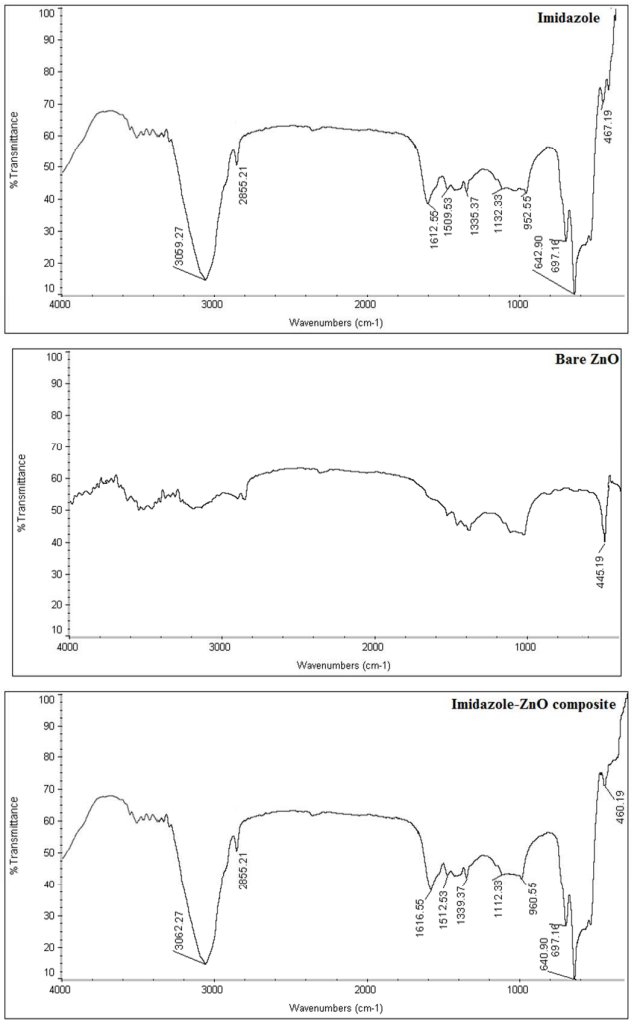

Figure 8. FT-IR spectra of imidazole, bare pristine ZnO and imidazole–ZnO composite

3.5. Evidence for linkage

Although there are three basic sites in the imidazole, the azomethine nitrogen is involved in the binding process with ZnO nanoparticles. This is because of the high electron density at the azomethine nitrogen. In order to prove the higher electron density at azomethine nitrogen, we have performed DFT calculation to get the molecular electrostatic potential (MEP) for imidazole, bare ZnO and imidazole-ZnO composite. The MEP map (Figure 9) shows that nitrogen atoms represent the most negative potential region (dark red). The predominance of green region in the MEP surface corresponds to a potential halfway between the two extremes red and dark blue colour.

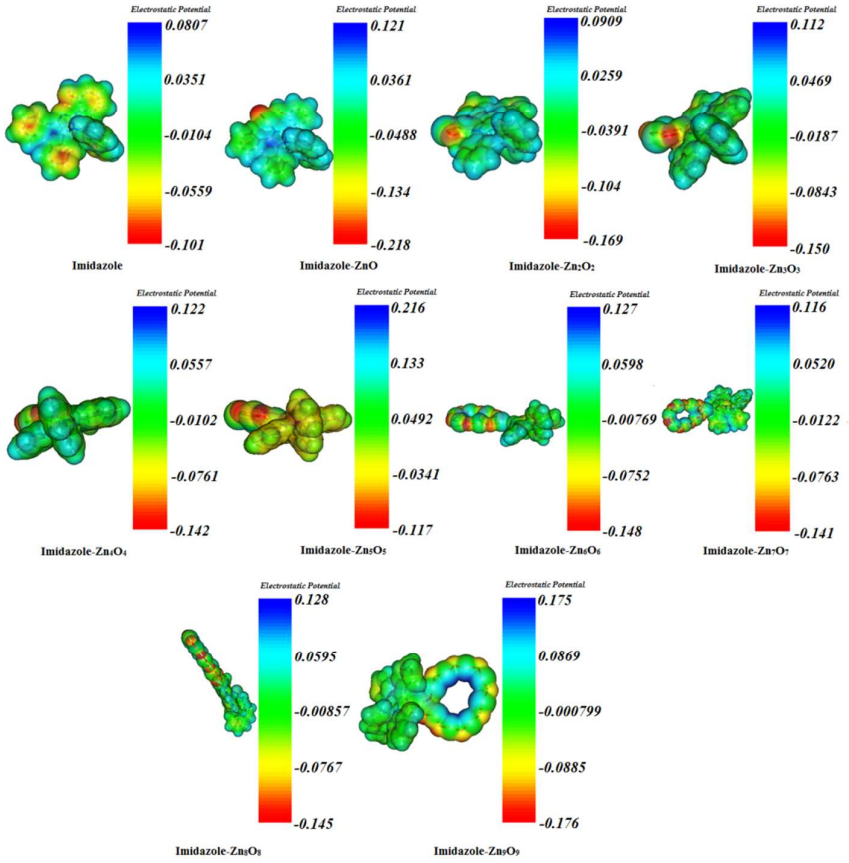

Figure 9. Molecular electrostatic potential (MEP) diagram of imidazole–Zn_nO_n composites

3.6. Electronic properties of ZnO clusters and imidazole-ZnO composites

To get a better insight on the nature of binding of the imidazole with the ZnO surface, DFT calculations have been made with Zn_nO_n (n = 1-10) clusters of different geometries. ZnO, Zn_2O_2, Zn_3O_3, Zn_4O_4 (R), Zn_4O_4 (W), Zn_5O_5, Zn_6O_6 (R), Zn_6O_6 (C), Zn_7O_7 (R), Zn_8O_8 (R), Zn_9O_9, (R) and $Zn_{10}O_{10}$ (C) are the clusters used for the calculation. The optimized geometries of imidazole, bare Zn_nO_n clusters and their corresponding imidazole-ZnO composite are shown in Figure 10 and the optimization parameters, energy gap (E_g) and binding energies (E_b) are given in Table 1. In the optimized bare ZnO clusters, the Zn–O bond length varies from 1.87 Å to 1.99 Å. Due to the adsorption of imidazole on bare ZnO, the surface structure of the ZnO is slightly distorted. Thus the surface Zn–O bond lengths in the imidazole-ZnO composite are expanded by a smaller amount (2.01 Å to 2.07 Å). The Zn–

O bonds are mainly ionic in nature and charge transfer occurs from zinc to more electronegative oxygen atoms. This charge transfer occurs in greater amounts in the surface region.

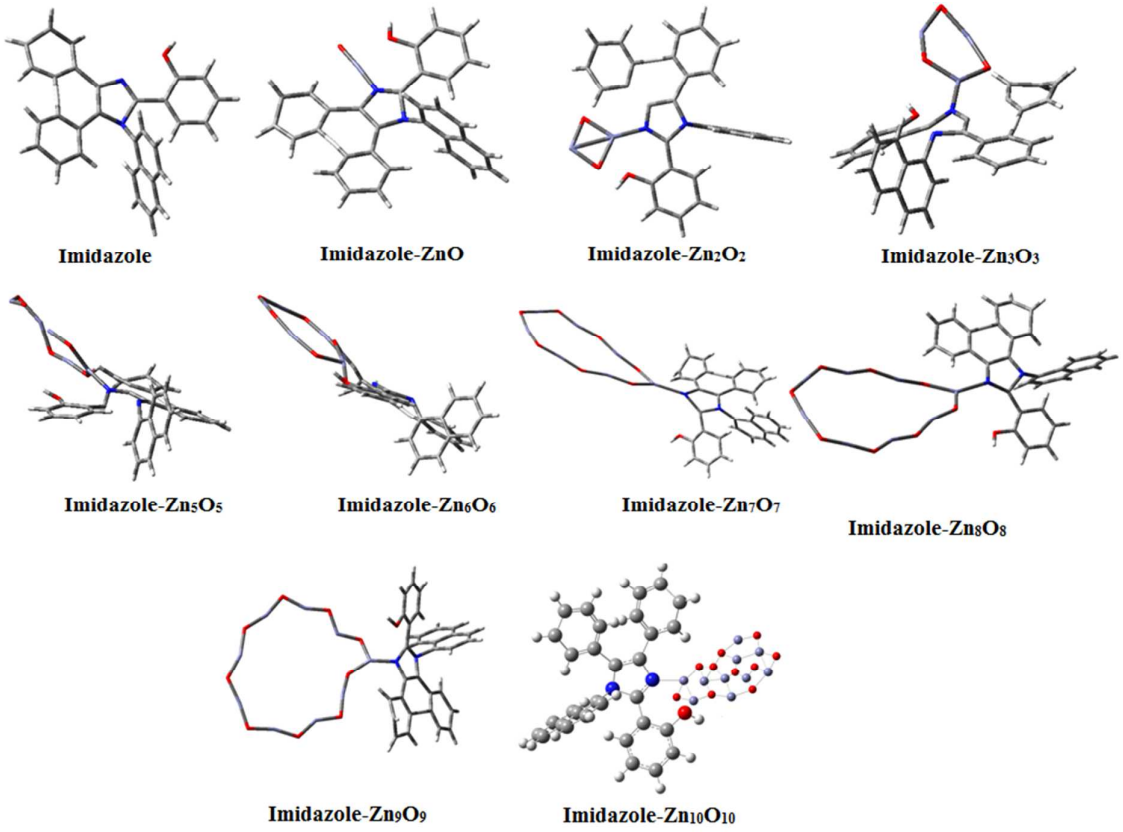

Figure 10. Optimized structures of imidazole–Zn_nO_n composites

The binding energy (E_b) of ZnO clusters have been calculated by using the equation, E_b = (n E_{Zn} + n E_O – E_{ZnO})/n, where n is the number of ZnO molecules in the cluster. The binding interactions between imidazole with the ZnO clusters have been analysed by binding energy, $E_b = E_{composite} - (E_{ZnO} + E_{imidazole})$, where $E_{composite}$ is the total energy of imidazole adsorbed on the ZnO, E_{ZnO} and $E_{imidazole}$ are the energies of the ZnO clusters and imidazole, respectively. The calculated results show that the binding energies (E_b) of the ring ZnO cluster is larger than those of cage geometries. From the optimized parameters and binding energies it is confirmed that the zinc atom of ZnO clusters prefer to bind through the azomethine nitrogen atom of imidazole (N- site). There is an overlap occurring between the

d-orbital of zinc and azomethine nitrogen atom which lead to a greater binding energy for N-site [40]. The covalent forces play a key role in deciding the strength of the interaction [41]. The energy gap of the ZnO clusters was calculated from the total densities of states (DOS) which is shown in Figure 11.

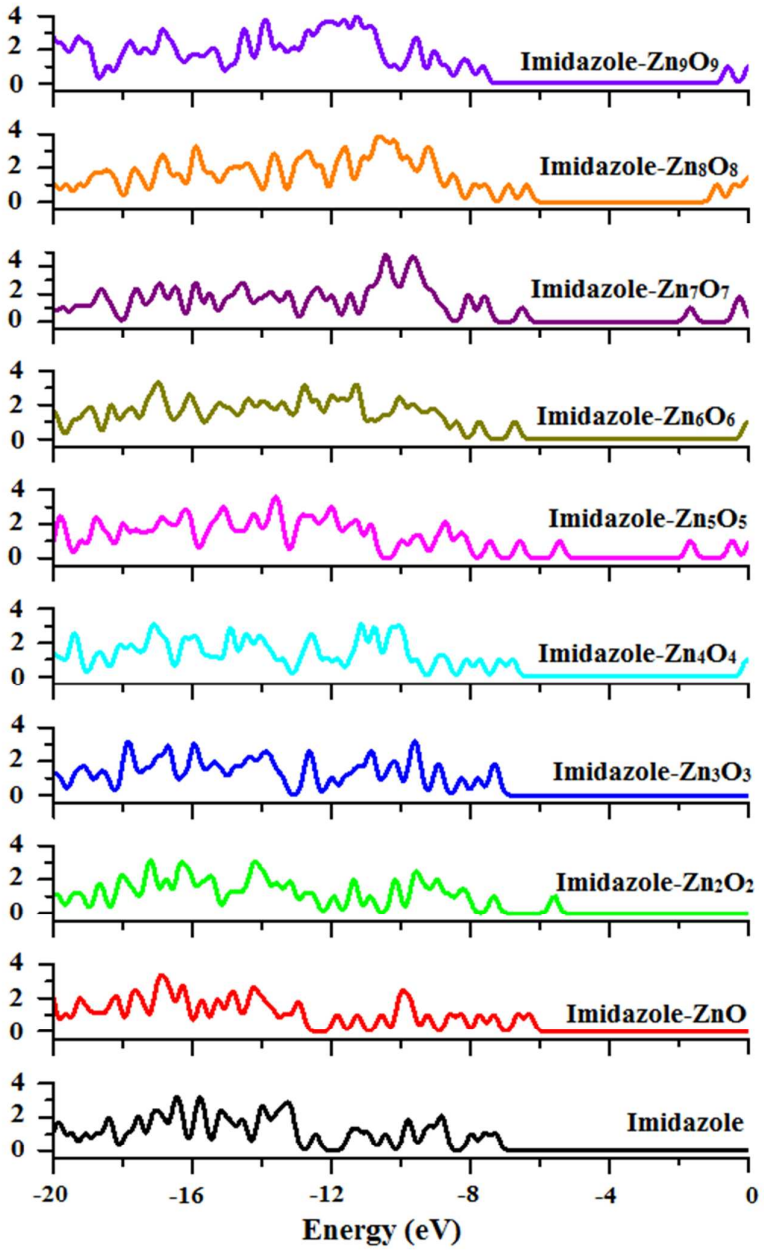

Figure 11. Density of state-plots for imidazole and imidazole–Zn_nO_n composites

To have an understanding of the extent of fractional charge transfer from imidazole to ZnO clusters, we have shown the Mulliken charges of the atoms of imidazole–ZnO composites in Tables S1 & S2. The MEP diagram, optimised geometries, DOS and HOMO-LUMO plots are given in Figures 9-12, respectively. For ZnO clusters the oxygen atom exhibits negative charge, which are donor atoms; zinc atom exhibits a positive charge, which is an acceptor atom. In imidazole–ZnO composite, the zinc atom exhibits a more positive charge and the azomethine nitrogen atom exhibits a more negative charge, these two atoms favor the weak interaction of Zn–N bond. In both bare ZnO clusters and imidazole-ZnO composites, all hydrogen atoms have positive charges. The values of the charge transfer give us some understanding of the character of the imidazole–ZnO interactions and also the nature of imidazole adsorption on the ZnO clusters.

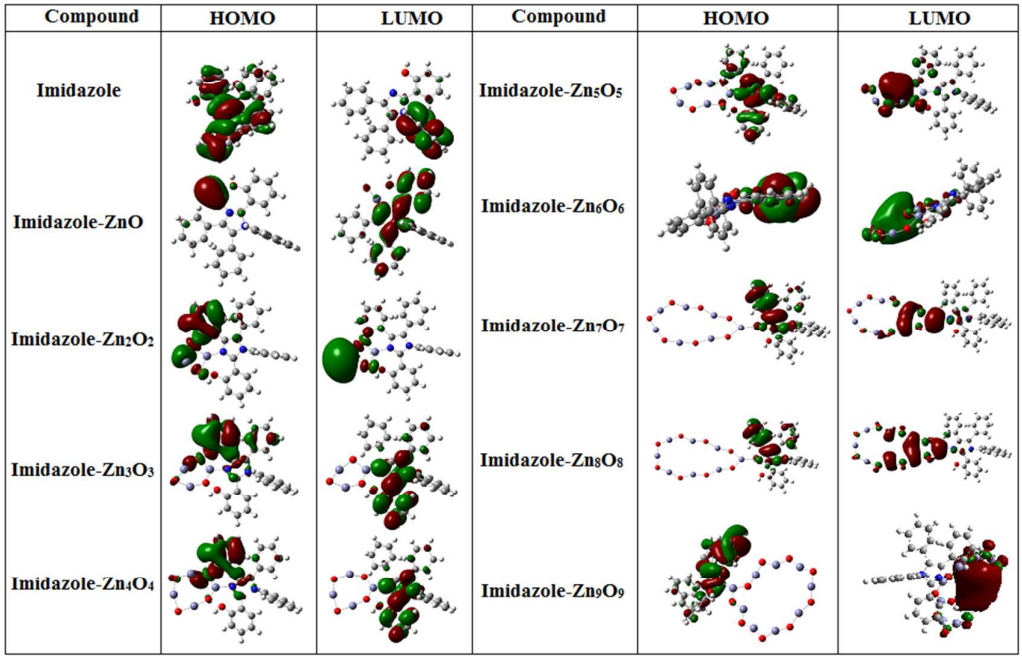

Figure 12. HOMO-LUMO contour maps for imidazole and imidazole–Zn_nO_n composites

The detailed calculated values of the binding energies for imidazole with different possible attacking sites to the ZnO are summarized in Table 1. The binding energy values suggest that the most preferred attacking site for imidazole to the ZnO surface is azomethine

nitrogen atom (N site). The equilibrium Zn–N bond length confirms the interaction regime for covalent forces. The HOMO–LUMO analysis explains the charge transfer taking place within the imidazole–ZnO composites. Usually the clusters with larger HOMO–LUMO gaps are more stable and chemically inert [42]. The above observation shows that the charge transfer occurs in the imidazole–Zn_nO_n (R) composite are faster than the same in other composites. The calculation results show that the ring structures of Zn_nO_n where n = 5-10 are the most stable geometries [43, 44]. All these results show that for both bare Zn_nO_n clusters and imidazole- Zn_nO_n composites, the ring structure is more stable for n = 1- 9 but when n = 10, the energy decrease and the bond angles of Zn-$\widehat{O}$-Zn and O-$\widehat{Zn}$-O also reach an extreme and so the ring structures no longer exist. Furthermore, the calculation shows that the Zn_9O_9 cluster less prefers the 2D ring geometry whereas the larger cluster with n = 10 is stabilized in 3D structure; ring to cage structural cross over takes place between Zn_9O_9 and $Zn_{10}O_{10}$ clusters. The Zn_9O_9 cluster is structurally distorted from planner geometry (D_{9h} symmetry) to zig-zag ring (C1 symmetry). Hence, the Zn_9O_9 clusters is the onset of 2D to3D structural cross over in ZnO clusters and the structural zig-zag distortion of Zn_9O_9 is attributed to the behavior of Zn-$\widehat{O}$-Zn bond angle. Because of the ionic Zn-O bonding, the valence electronic shell is mainly localized on oxygen nuclei while the zinc nuclei act as the localized positive charge centers and the presence of two lone pairs of electrons in the valence shell of oxygen prevents the linear configuration of Zn-O-Zn chains. In the perfect planar Zn_9O_9 structure, O-$\widehat{Zn}$-O is expected to be 135^o but the obtained zig-zag structural distortion reduces the O-$\widehat{Zn}$-O to about 124^o. For larger cluster (n = 10) zig-zag structural distortion with O-$\widehat{Zn}$-O angle of 124^o was obtained. The calculated dipolement of imidazole-Zn_6O_6(16.2), imidazole-Zn_7O_7(21.4), imidazole-Zn_8O_8(23.0) and imidazole-Zn_9O_9(11.7) .The decrease of dipolemoment of imidazole-Zn_9O_9 composite is due to the distortion from planner geometry (D_{9h} symmetry) to zig-zag ring (C1 symmetry). For smaller clusters, the ring structures with

smaller bond lengths and stronger single bond energies were obtained when compared with the cage structures because in 3D structures the atoms are more coordinated, containing more number of bonds and hence the valence electrons are divided into more bonds and gets weaker. In the smaller clusters, the number of bonds is less and the individual bond energy determines the stability. Increase of the cluster size enhances the coordination number and at some point (n = 10) a ring to cage structural transition occurs. The first 3D cluster $Zn_{10}O_{10}$ favors an intermediate configuration between the ring and cage structures which is composed of two Zn_5O_5 ring structures. The energy gap of ring clusters are larger than 2 eV while the cage clusters exhibit lower energy gap (< 2.0 eV) which shows that the energy gap is mainly sensitive to the cluster geometry and not to the cluster size.

Table 1. E_{HOMO}, E_{LUMO}, energy gap (E_g), distance Zn–N (A°), binding energies (E_b), optimised energies (E) and dipolemoments of imidazole– ZnO composites along with ZnO clusters

Compound	E_{HOMO} (eV)	E_{LUMO}(eV)	E_g/E_b (eV)	E_b (eV)		Zn–N	D
				N-site	O-site		
ZnO	-6.23	-3.55	2.68/5.89				1.26
Zn_2O_2	-6.0	-3.69	2.29/6.10	-	-	-	0.00
Zn_3O_3	-6.83	-3.11	3.72/7.12	-	-	-	0.01
Zn_4O_4 (R)	-6.84	-2.85	2.98/7.70	-	-	-	0.65
Zn_4O_4 (W)	-6.12	-3.86	2.24/7.19	-	-	-	3.21
Imidazole	-4.82	-1.12	3.70	-	-	-	3.37
Imidazole - ZnO	-4.32	-2.82	1.50	6.58	2.01	2.06	15.06
Imidazole - Zn_2O_2	-4.02	-2.21	1.81	7.89	2.91	2.07	7.26
Imidazole - Zn_3O_3	-4.10	-2.71	1.39	7.10	3.69	2.04	10.2
Imidazole - Zn_4O_4 (R)	-3.89	-2.63	1.26	8.12	3.72	2.01	9.28
Imidazole - Zn_4O_4 (W)	-3.52	-2.56	0.96	7.73	3.19	2.02	9.80

3.7. Imidazole as Zn^{2+} ion sensor

The synthesised imidazole was tested for sensing different metal ions such as Zn^{2+}, Cd^{2+}, Cu^{2+}, Ni^{2+}, Co^{2+}, Mg^{2+} and Mn^{2+} in aqueous alcoholic solution. The results show that the imidazole act as an efficient sensor for Zn^{2+}. The three absorption bands of imidazole molecule at 311, 285 and 227 nm are assigned to $^1(\pi - \pi^*)$ transition corresponding to Platt's notations ^1L_b, ^1L_a and ^1B_a in the excited states. This shows that the superposition of the bands corresponding to the donor and acceptor subunits which seem to be only slightly perturbed by their interactions [45, 46]. The low energy absorption of the imidazole containing naphthyl as an electron acceptor indicates the presence of additional charge transfer singlet states. The absorption around 386 and 417 nm can be assigned to metal → ligand charge transfer (MLCT) and ligand → ligand charge transfer (LLCT) for imidazole -Zn^{2+} complex. The high energy absorption at 242 and 276 nm are from ligand π-π* transitions. The absorbance of imidazole is found to be very sensitive to the presence of even submicromolar traces of zinc ion. Binding constant K was calculated according to the Benesi-Hildebrand equation, $1/(A-A_0) = 1/\{K(A_{max}-A_0)\ [Zn^{2+}]_n\}+1/[A_{max}-A_0]$, here A_o is the absorbance of receptor in the absence of Zn^{2+}, A is the absorbance recorded in the presence of Zn^{2+}, A_{max} is absorbance in presence of added $[Zn^{2+}]_{max}$ and K is the binding constant (M^{-1}). The binding constant (1.78×10^7) is determined from the slope of the plot of $1/(A-A_0)$ against $1/[\ Zn^{2+}]$, confirming 1:1 binding [47].

Addition of even trace of zinc ion results in increase of the emission intensity of imidazole. The affinity of imidazole with other metal ions, such as Cd^{2+}, Cu^{2+}, Ni^{2+}, Co^{2+}, Mg^{2+} and Mn^{2+} is significantly lower than that for Zn^{2+} (Figure 13). The binding constant has been obtained from the following equation, $1/(F - F_0) = 1/(F - F_0) + 1/\ K\ (F - F_0)$ [imidazole], where K is the binding constant, F_0 is the fluorescence intensity of the bare imidazole derivative, F is the fluorescence intensity of the composite. A linear relationship

was obtained by the plot of $1/(F - F_0)$ and the reciprocal concentration of Zn^{2+} ion. The binding constant (1.99×10^7) for imidazole -Zn^{2+} complex is in agreement with that obtained from the absorbance results. Different binding constants calculated are shown in Table 2. The emission intensity of imidazole is almost unaffected by the presence of Li^+, Na^+ and K^+ ions and the weaker effect of these ions shows less affinity of imidazole toward those ions.

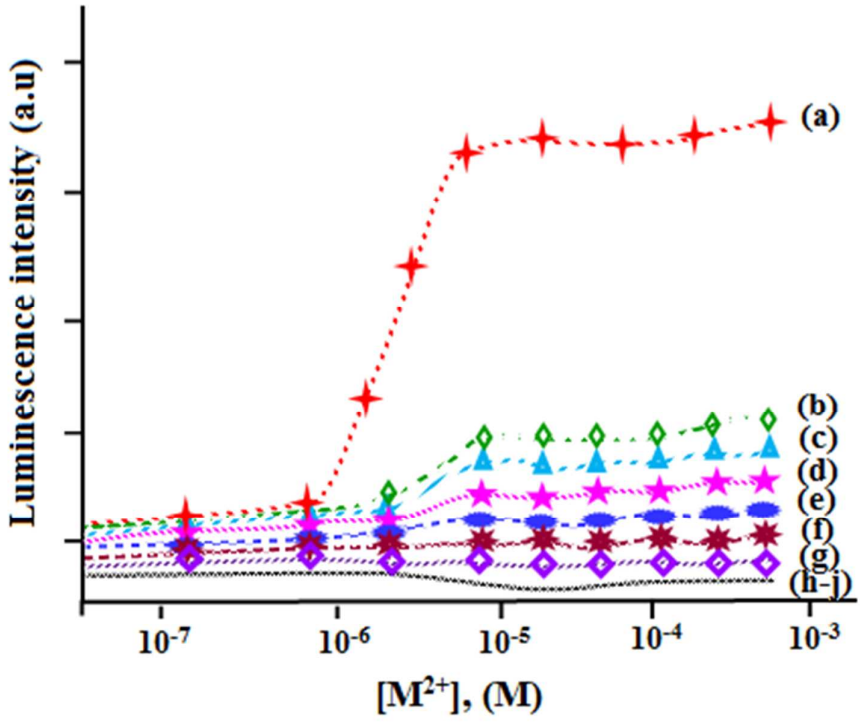

Figure 13. Relative emission intensities of a solution of $1x10^{-5}$ M of imidazole in dioxane in the presence of different metal ions: (a) $Zn(NO_3)_2$, (b) $Cu(NO_3)_2$, (c) $Cd(NO_3)_2$, (d) $Co(NO_3)_2$, (e) $Mn(NO_3)_2$, (f) $Ni(NO_3)_2$, (g) $Mg(NO_3)_2$, (h) $LiNO_3$, (i) $NaNO_3$ and (j) KNO_3 with different concentrations of 0 M, 9.85×10^{-8} M, 4.88×10^{-7} M, 8.90×10^{-7} M, 3.00×10^{-6} M, 4.86×10^{-6} M, 7.45×10^{-6} M, 9.42×10^{-6} M

Table 2. Binding constant (***K***) for various imidazole-metal ion complexes

Ion	K (M^{-1})
Zn^{2+}	2.0×10^{7}
Cu^{2+}	1.9×10^{6}
Cd^{2+}	9.0×10^{5}
Co^{2+}	3.6×10^{5}
Mn^{2+}	2.6×10^{4}
Ni^{2+}	2.4×10^{5}
Mg^{2+}	2.8×10^{3}
Li^{+}	Less sensitive
Na^{+}	Less sensitive
K^{+}	Less sensitive

The enhancement in fluorescence intensity of imidazole on interaction with Zn^{2+} ion may be explained on the basis of photoinduced electron transfer (PET) mechanism [48] between imidazole and Zn^{2+} ion. The Zn^{2+} ion binds to imidazole via lone pair of electron of the azomethine nitrogen atom and recognition group of the imidazole moiety. The PET process occurs due to the transfer of electron from the lone pair electron on nitrogen atom of the imidazole moiety to the LUMO of the fluorophore. Binding of Zn^{2+} to imidazole through the nitrogen atom lone pair will obviously hinder the PET process leading to fluorescence intensity enhancement of imidazole on interaction with Zn^{2+} ion (Scheme 1).The observation that the synthesised imidazole act as an effective sensor for Zn^{2+} ion than the listed other ions supports the enhancement of emission of imidazole by nanocrystalline ZnO;the chemical affinity of the imidazole to Zn^{2+} ion could be the reason for the observed fluorescence enhancement.

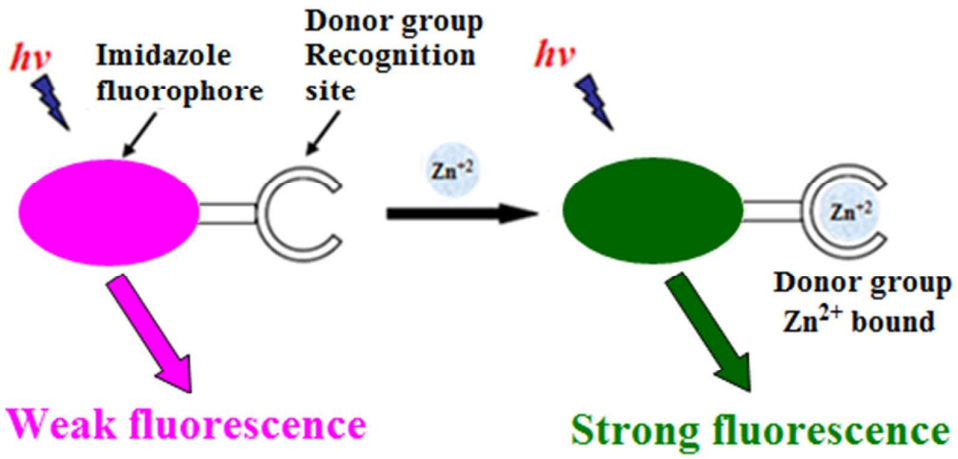

Scheme 1. Metal ion sensing by fluorescent photoinduced electron transfer (PET) indicators

3.8. HOMO-LUMO energies

Orbital energy level diagram for the free imidazole and imidazole - Zn^{2+} complex by DFT analysis shows that the PET of imidazole is due to the presence of lone pair electron on azomethine nitrogen which behaves as a quencher and also as the binding site for metal ion (Scheme 2). The energies of the LUMO, HOMO, HOMO-1, HOMO-2 and any other relevant orbital of the energy minimized systems were extracted from the calculations and presented in Figure 14 for the free imidazole and imidazole -Zn^{2+} complex, respectively. Fluorescence of free imidazole originates from its orbital structure in which two π-orbitals (HOMO and HOMO-1) of the imidazole ring are situated between two π -orbitals (HOMO-2 and LUMO) of the naphthyl moiety. The two π-orbitals of the imidazole ring are located between the two π-orbitals that participate in photoexcitation and emission which is indicative of a PET system. In contrast, the lone pair of nitrogen atom of imidazole ring is at a lower energy than HOMO-2. This explains the low fluorescence efficiency found for the free host. In the imidazole -Zn^{2+} complex, both the HOMO and LUMO π-orbitals participate in the photoexcitation and emission processes. The π-orbitals of imidazole ring located at HOMO-1 and HOMO-2 are low in energy than HOMO so that the emission intensity is enhanced.

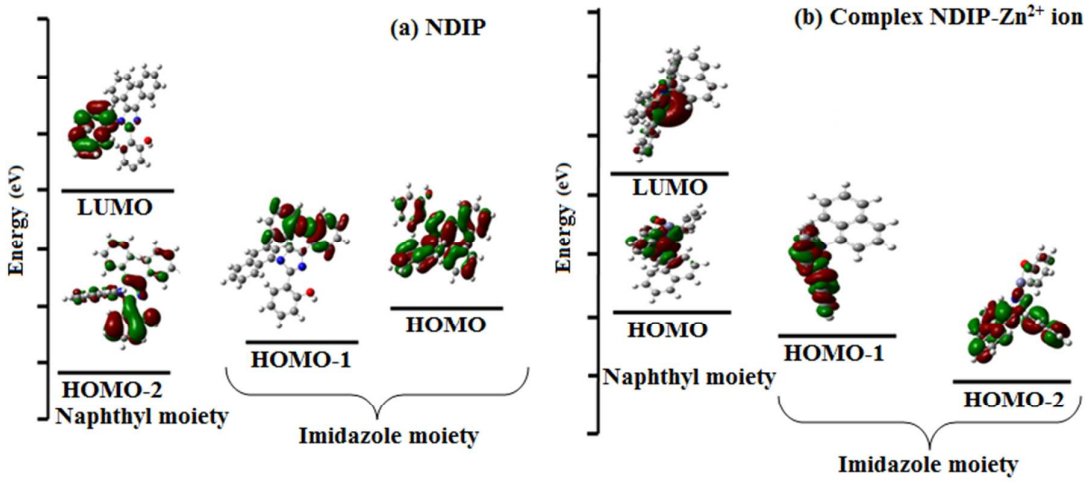

Figure 14. (**a**) Orbital energy diagram for imidazole (Gaussian 03software package, B3LYP/6-31G (d,p)); (**b**) Orbital energy diagram for composite imidazole -Zn^{2+} ion (Gaussian 03 software package, B3LYP/6-31G (d,p))

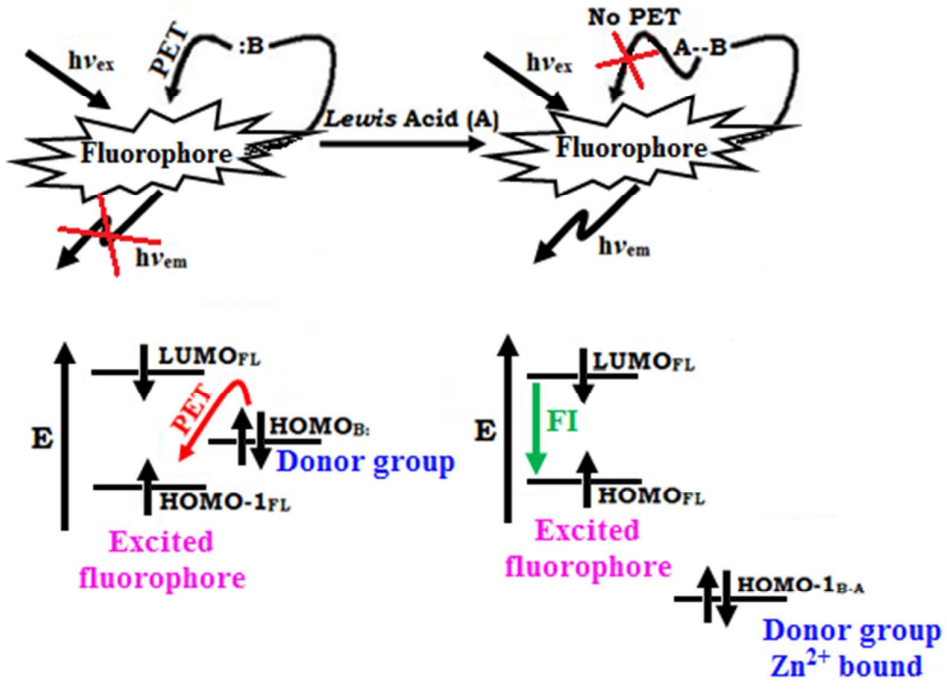

Scheme 2. Energy diagram of PET based sensing

4. Conclusion

The enhanced absorbance and emission intensity observed with the dispersed semiconductor nanoparticles is due to the formation of the composite. Fluorescent enhancement has been explained and apparent binding constant has been calculated based on photoinduced electron transfer mechanism. The negative ΔG_{et} value reveals the electron transfer process is thermodynamically favourable. The interaction between the imidazole and ZnO clusters is dominated by the hybridization between *d*-orbitals of zinc and nitrogen atoms and this determines the strength of interaction imidazole with ZnO. On adsorption of the imidazole on the ZnO clusters modifies the electronic properties of the ZnO clusters and the HOMO–LUMO analysis confirms the occurrence of charge transfer. Mulliken charge distribution shows that zinc atom exhibits more positive charge and the azomethine nitrogen atom exhibits a more negative charge. These two atoms form the weak Zn–N bond (N-site) in imidazole–ZnO composite. The calculation reveals that reduction in the energy gap for imidazole- ZnO composite when compared to bare ZnO and imidazole. The Zn_9O_9 cluster less prefers the 2D ring geometry whereas the larger cluster with n = 10 is stabilized in 3D structure; ring to cage structural cross over takes place between Zn_9O_9 and $Zn_{10}O_{10}$ clusters. A new imidazole based photoelectron transfer system shows potential affinity toward Zn^{2+} ion and its imidazole -Zn^{2+} complex is found to be more fluorescent than free imidazole.

5. Acknowledgments

One of the authors Prof. J. Jayabharathi is thankful to DST (No. SR/S1/IC-73/2010), DRDO (NRB-213/MAT/10-11) and CSIR (No. 3732/NS-EMRII) for providing funds to this research study.

References

[1] (a) L. Vayssieres, K. Keis, A. Hagfeldt and S.E. Lindquist, *Chem. Mater.,* 2001, **13**, 4395-4398; (b) J.A. Rodriguez, T. Jirsak, J. Dvorak, S. Sambasivan and D. Fischer, *J. Phys. Chem. B.,* 2000, **104**, 319-328.

[2] (a) M. Bruchez Jr, M. Moronne, P. Gin, S. Weiss and A.P. Alivisatos, *Science,* 1998, **281**, 2013-2016; (b) I.L. Medintz, H.T. Uyeda, E.R. Goldman and H. Mattoussi, *Nat. Mater.,* 2005, **4**, 435-446; (c) A.R. Clapp, I.L. Medintz, J.M. Mauro, B.R. Fisher, M.G. Bawendi and H. Mattoussi, *J. Am. Chem. Soc.,* 2004, **126**, 301-310; (d) B.P. Aryal and D.E. Benson, *J. Am. Chem. Soc.,* 2006, **128**, 15986-15987.

[3] P.D. Beer and P.A. Gale, *Angew. Chem., Int. Ed.,* 2001, **40**, 486-516.

[4] A. Nel, T. Xia, L. Ma¨dler and N. Li, *Science,* 2006, **311**, 622-627.

[5] S. Rakshit and S. Vasudevan, *J. Phys. Chem. C.,* 2008, **112**, 4531-4537.

[6] D. S. Bohle and C. J. Spina, *J. Am. Chem. Soc.,* 2007, **129**, 12380-12381.

[7] H. M. Xiong, Y. Xu, Q.G. Ren and Y.Y. Xia, *J. Am. Chem. Soc.,* 2008, **130**, 7522-7523.

[8] H. Wang, D. Wingett, M.H. Engelhard, K. Feris, K.M. Reddy, P. Turner, J. Layne, C. Hanley, J. Bell, D. Tenne, C. Wang and A. Punnoose, *J. Mater. Sci.: Mater. Med.,* 2009, **20**, 11-22.

[9] S. Dhobale, T. Thite and S. L. Laware, *J. Appl. Phys.,* 2008, **104**, 094907.

[10] C. Hanley, J. Layne and A. Punnoose, *Nanotechnology,* 2008, **19**, 295103.

[11] K.M. Reddy, K. Feris, J. Bell, D.G. Wingett, C. Hanley and A. Punnoose, *Appl. Phys. Lett.,* 2007, **90**, 213902.

[12] A. S. Barnard, *Nat. Nanotechnol.,* 2010, **5**, 271-274.

[13] J. Musarrat, Q. Saquib, A. Azam and S.A.H. Naqvi, *Int. J. Nanopart.,* 2009, **2**, 402-415.

[14] T. Thomas, K. Thomas, N. Sadrieh, N. Savage, P. Adair and R. Bronaugh, *Toxicol. Sci.,* 2006, **91**, 14-19**.**

[15] (a) G. Li, J.Li, C. Zhang, Y. Hu, X. Li, J. Chu, W.Huang and D.Wu, *J. Phys. Chem. C.,* 2009, **113**, 21338-21341; (b) K. Kotsis and V. Staemmler, *Phys. Chem. Chem. Phys.,* 2006, **8**, 1490-1498; (c) J.M. Matxain, J.E. Fowler and J.M. Ugalde, *Physical Review A,* **62**, 053201; (d) R. Steudel, Y. Steudel and M.W. Wong, *Chem. Eur. J.,* 2008, **14**, 919-932; (e) N. Rossler, K. Kotsis and V. Staemmler, *Phys. Chem. Chem. Phys.,* 2006, **8**, 697-706; (f) M. Zhao, Y. Xia, Z. Tanb, X. Liu and L. Mei, *Phys. Lett., A*. 2007, **372**, 39-43; (g) C. Wang, S. Xu, L. Ye, W. Lei and Y. Cui., *J. Mol. Model.,* 2011, **17**, 1075-1080; (h) F.D. Angelis and L. Armelao, *Phys. Chem. Chem. Phys.,* 2011, **13**, 467-475; (i) X. Cheng, F. Li and Y. Zhao, *J. Mol. Struct. Theochem.,* 2009, **894**, 121-127; (j) A. Choudhury, S. Neeraj, S. Natarajan and C.N.R. Rao, *Dalton Trans.,* 2002, 1535-1538.

[16] A. K. Jissy and A. Datta, *J. Phys. Chem. Lett.,* 2014, **5**, 154-166.

[17] T. Wang, Y. Hu, L. Zhang, L. Jiang, Z. Chen and N.Y. He, *Nano Biomed. Eng.,* 2010, **2**, 31-46.

[18] S. H. Chen, Y. X. Ji, Q. Lian, Y. L. Wen, H. B. Shen and N. Q. Jia, *Nano Biomed. Eng.,* 2010, **2**, 15-23.

[19] S. L. Bechara, A. Judson and K. C. Popat, *Biomaterials,* 2010, **31**, 3492-3501.

[20] Y. Q. Li, Z. Y. Li, X. P. Zhou and P. Yang, *Nano Biomed. Eng.,* 2010, **2**, 19-24.

[21] V. Shewale, P. Joshi, S. Mukhopadhyay, M. Deshpande, R. Pandey, S. Hussain and S. P. Karna, *J. Phys. Chem. C,* 2011, **115**, 10426-10430.

[22] P. Joshi, V. Shewale, R. Pandey, V. Shanker, S. Hussain and S.P. Karna, *Phys. Chem. Chem. Phys.,* 2011,**13**, 476-479.

[23] (a) N.B. Sankaran, S. Banthia, S. Das and A. Samanta, *New. J. Chem.,* 2002, **26**, 1529-1531; (b) D. Cordier and P.R. Coulet, *Perkin Trans.,* 1994, **2**, 891-894; (c) R. Krauss, H.G. Weinig, M. Seydack, J. Bendig and U. Koert, *Angew. Chem., Int. Ed.,* 2000, **39**, 1835-1837; (d) F. Pina, M.A. Bernardo and E. Garcia-Espana, *Eur. J. Inorg. Chem.,*

2000, **10**, 2143-2157; (e) S. Ressalan and C.S.P. Iyer, *J. Lumin.,* 2005, **111**, 121-129; (f) A.P. de Silva, H.Q.N. Gunaratne, T. Gunnlaugsson, A.J.M. Huxley, C.P. McCoy, J.T. Rademacher and T.E. Rice, *Chem. Rev.,* 1997, **97**, 1515-1566.

[24] (a) Y. Liu, Z.Y. Duan, H.Y. Zhang, X.L. Jiang and J.R. Han, *J. Org. Chem.,* 2005, **70**, 1450-1455; (b) S.J.K. Pond, O. Tsutsumi, M. Rumi, O. Kwon, E. Zojer, J.L. Bredas, S.R. Marder and J.W. Perry, *J. Am. Chem. Soc.,* 2004, **126**, 9291-9306; (c) A.J. Pearson and W.J. Xiao, *J. Org. Chem.,* 2003, **68**, 5369-5376.

[25] (a) J.H. Bu, Q.Y. Zheng, C.F. Chen and Z.T. Huang, *Org. Lett.,* 2004, **6**, 3301-3304; (b) Y. Nakahara, T. Kida, Y. Nakatsuji and M. Akashi, *Org. Biomol. Chem.,* 2005, **3**, 1787-1794; (c) H. Tuncer and C. Erk, *Talanta,* 2005, **65**, 819-823; (d) Y. Liu, Z.Y. Duan, Y. Chen, J.R. Han and C. Lu, *Org. Biomol. Chem.,* 2004, **2**, 2359-2364; (e) G. McSkimming, J.H.R. Tucker, H. Bouas-Laurent, J.P. Desvergne, S.J. Coles, M.B. Hursthouse and M.E. Light, *Chem. Eur. J.,* 2002, **8**, 3331-3342; (f) N.B. Sankaran, S. Nishizawa, M. Watanabe, T. Uchida and N. Teramae, *J. Mater. Chem.,* 2005, **15**, 2755-2761.

[26] (a) H. Salman, Y. Abraham, S. Tal, S. Meltzman, M. Kapon, N. Tessler, S. Speiser and Y. Eichen, *Eur. J. Org. Chem.,* 2005, **11**, 2207-2212; (b) J. Kang and J. Kim, *Tetrahedron Lett.,* 2005, **46**, 1759-1762; (c) B. Liu and H. Tian, *Chem. Lett.,* 2005, **34**, 686-687; (d) Y. Bai, B.G. Zhang, J. Xu, C.Y. Duan, D. B. Dang, D.J. Liu and Q.J. Meng, *New J. Chem.,* 2005, **29**, 777-779; (e) H. Kim and J. Kang, *Tetrahedron Lett.,* 2005, **46**, 5443-5445; (f) P. Piatek, V.M. Lynch and J.L. Sessler, *J. Am. Chem. Soc.,* 2004, **126**, 16073-16076; (g) T. Ghosh, B.G. Maiya and M.W. Wong, *J. Phys. Chem. A.,* 2004, **108**, 11249-11259; (h) P. Anzenbacher, A.C. Try, H. Miyaji, K. Jursikova, V.M. Lynch, M. Marquez and J.L. Sessler, *J. Am. Chem. Soc.,* 2000, **122**, 10268-10272; (i) G. Xu and M.A. Tarr, *Chem. Commun.,* 2004, **9**, 1050-1051; (j) C.F. Chen and Q.Y.

Chen, *Tetrahedron Lett.,* 2004, **45**, 3957-3960; (k) C.B. Black, B. Andrioletti, A.C. Try, C. Ruiperez and J.L. Sessler, *J. Am.Chem. Soc.,* 1999, **121**, 10438- 10439.

[27] (a) T. Gunnlaugsson, A.P. Davis, J.E. O'Brien and M. Glynn, *Org. Biomol. Chem.,* 2005, **3**, 48-56; (b) J.L. Wu, Y. B. He, Z.Y. Zeng, L.H. Wei, L.Z. Meng and T.X. Yang, *Tetrahedron,* 2004, **60**, 4309-4314; (c) D. Reyman, M.J. Tapia, C. Carcedo and M.H. Vinas, *Biophys. Chem.,* 2003, **104**, 683-696; (d) T. Gunnlaugsson, A.P. Davis, J.E. O'Brien and M. Glynn, *Org. Lett.,* 2002, **4**, 2449-2452; (e) L. Fabbrizzi, M. Licchelli, L. Parodi, A. Poggi and A. Taglietti, *Eur. J. Inorg. Chem.,* 1999, **1**, 35-39.

[28] (a) S.A. de Silva, K.C. Loo, B. Amorelli, S.L. Pathirana, M. Nyakirang'ani, M. Dharmasena, S. Demarais, B. Dorcley, P. Pullay and Y.A. Salih, *J. Mater. Chem.,* 2005, **15**, 2791-2795; (b) E. Arunkumar and A. Ajayaghosh, *Chem. Commun.,* 2005, **5**, 599-601; (c) A.P. de Silva, H.Q.N. Gunaratne and C.P. McCoy, *Chem. Commun.,* 1996, **21**, 2389-2393.

[29] I. Grabchev, J. M. Chovelon and X. Qian, *New. J. Chem.,* 2003, **27**, 337-340.

[30] (a) T. Gunnlaugsson, H.D.P. Ali, M. Glynn, P.E. Kruger, G.M. Hussey, F.M. Pfeffer, C.M.G. Santos and J. Tierney, *J. Fluoresc.,* 2005, **15**, 287-299; (b) T. Gunnlaugsson, A.P. Davis, G.M. Hussey, J. Tierney and M. Glynn, *Org. Biomol. Chem.,* 2004, **2**, 1856-1863; (c) T. Gunnlaugsson, P.E. Kruger, T.C. Lee, R. Parkesh, F.M. Pfeffer and G.M. Hussey, *Tetrahedron Lett.,* 2003, **44**, 6575-6578; (d) T. Gunnlaugsson, A.P. Davis and M. Glynn, *Chem. Commun.,* 2001, **24**, 2556-2557; (e) Y. Kubo, M. Kato, Y. Misawa and S. Tokita, *Tetrahedron Lett.,* 2004, **45**, 3769-3773.

[31] (a) Z. Ebru Seckin and M. Volkan, *Anal. Chim. Acta.,* 2005, **547**, 104-108; (b) T. Sahu, S.K. Pal, T. Misra and T. Ganguly, *J. Photochem. Photobiol. A.,* 2005, **171**, 39-50; (c) N. Soh, O. Sakawaki, K. Makihara, Y. Odo, T. Fukaminato, T. Kawai, M. Irie and T. Imato, *Bioorg. Med. Chem.,* 2005, **13**, 1131-1139; (d) X. Guo, D. Zhang, D. Zhang,

Y. Guan and D. Zhu, *Chem. Phys. Lett.,* 2004, **398**, 93-97; (e) J. Nakanishi, M. Maeda and Y. Umezawa, *Anal. Sci.,* 2004, **20**, 273-278; (f) K. Sen and S. Basu, *Chem. Phys. Lett.,* 2004, **387**, 61-65; (g) Y. Gabe, Y. Urano, K. Kikuchi, H. Kojima and T. Nagano, *J. Am. Chem. Soc.,* 2004, **126**, 3357-3367; (h) E. Nakata, T. Nagase, S. Shinkai and I. Hamachi, *J. Am. Chem. Soc.,* 2004, **126**, 490-495; (i) S.K. Pal, T. Bhattacharya, T. Misra, R.D. Saini and T. Ganguly, *J. Phys. Chem. A.,* 2003, **107**, 10243-100251.

[32] (a) I. Leray, J.P. Lefevre, J.F. Delouis, J. Delaire and B. Valeur, *Chem. Eur. J.,* 2001, **7**, 4590-4598; (b) S.C. Burdette, G.K Walkup, B. Spingler, R.Y. Tsien and S.J. Lippard, *J. Am. Chem. Soc.,* 2001, **123**, 7831-7841.

[33] (a) C. Karunakaran, J. Jayabharathi and K. Jayamoorthy, *Spectrochim. Acta, Part A.,* 2013, **114**, 303-308; (b) C. Karunakaran, J. Jayabharathi and K. Jayamoorthy, *Spectrochim. Acta, Part A.,* 2013, **112**, 417-421; (c) C. Karunakaran, J. Jayabharathi, R. Sathishkumar and K. Jayamoorthy, *Spectrochim. Acta, Part A.,* 2013, **110**, 151-156; (d) C. Karunakaran, J. Jayabharathi, M. Venkatesh Perumal, V. Thanikachalam and P.K. Thakur, *J. Phys. Org. Chem.,* 2013, **26**, 386-406; (e) C. Karunakaran, J. Jayabharathi and K. Jayamoorthy, *Sensor Actuat B-Chem.,* 2013, **182**, 514-520; (f) C. Karunakaran, J. Jayabharathi, R. Sathishkumar and K. Jayamoorthy, *J. Lumin.,* 2013, **138**, 235-241; (g) C. Karunakaran, J. Jayabharathi, K. Jayamoorthy and P. Vinayagamoorthy, *J. Mol. Liq.,* 2013, **177**, 295-300; (h) C. Karunakaran, J. Jayabharathi, K. Jayamoorthy and P. Vinayagamoorthy, *J. Photochem. Photobiol A.,* 2012, **247**, 16-23; (i) C. Karunakaran, J. Jayabharathi, K. Jayamoorthy and K.Brindha Devi, *Sens. Actuators, B. Chem.,* 2012, **168**, 263-270; (j) C. Karunakaran, J. Jayabharathi, K. Jayamoorthy and K.Brindha Devi, *J. Fluoresc.,* 2012, **22**, 1047-1053; (k) C. Karunakaran, J. Jayabharathi, K. Jayamoorthy and K.Brindha Devi, *Spectrochim. Acta, Part A.,* 2012, **89**, 187-193.

[34] C. Karunakaran, P. Anilkumar and P. Gomathisankar, *Chem. Central Journal.,* 2011, **123**, 5:31.

[35] M.J. Frisch, G.W. Trucks, H.B. Schlegel, G.E. Scuseria, M.A. Robb, J.R. Cheeseman, V.G. Zakrzewski, J.A. Montgomery, R.E. Stratmann, J.C. Burant, S. Dapprich, J. M. Millam, A.D. Daniels, K.N. Kudin, M.C. Strain, O. Farkas, J. Tomasi, V. Barone, M. Cossi, R. Cammi, B. Mennucci, C. Pomelli, C. Adamo, S. Clifford, J. Ochterski, G.A. Petersson, P.Y. Ayala, Q. Cui, K. Morokuma, D.K. Malick, A.D Rabuck, K. aghavachari, J.B. Foresman, J. Cioslowski, J.V. Ortiz, B.B. Stefanov, G. Liu, A. Liashenko, P. Piskorz, I. Komaromi, R. Gomperts, R.L. Martin, D.J. Fox, T. Keith, M.A. Al-Laham, C.Y. Peng, A. Nanayakkara, C. Gonzalez, M. Challacombe, P.M.W. Gill, B.G. Johnson, W. Chen, M.W. Wong, J.L. Andres, M. Head-Gordon, E.S. Replogle, J.A. Pople, Gaussian 98; Gaussian, Inc.: Pittsburgh, PA, 2002.

[36] G.J. Kavarnos and N.J. Turro, *Chem. Rev.,* 1986, **86**, 401-449.

[37] S. Parret, F.M. Savary, J.P. Fouassier and P. Ramamurthy, *J. Photochem. Photobiol. A.,* 1994, **83**, 205-209.

[38] K. Kikuchi, T. Niwa, Y. Takahashi, H. Ikeda and T. Miyashi, *J. Phys. Chem.,* 1993, **97**, 5070-5073.

[39] (a) X. Wang, R. Zhang, C. Wu, Y. Dai, M. Song, S. Gutmann, F. Gao, G. Lv, J. Li, X. Li, Z. Guan, D. Fu and B. Chen, *J. Biomed. Mater. Res A.,* 2007, **80A**, 852-860; (b) S. Saha and P. Sarkar, *Phys. Chem. Chem. Phys.,* 2014, **16**, 15355-15366.

[40] J. Jayabharathi, V. Thanikachalam, M. Venkatesh Perumal and N. Srinivasan, *J. Fluoresc.,* 2012, **22**, 409-417.

[41] (a) C. Arunagiri, A. Subashini, M. Saranya and P. T. Muthiah, *Ind. J. Appl. Res.,* 2013, **3**, 78-84; (b) A.V. Kachynski, A.N. Kuzmin, M. Nyk, I. Roy and P.N. Prasad, *J. Phys. Chem. C.,* 2008, **112**, 10721-10724.

[42] B. Wang, S. Nagase, J. Zhao and G. H. Wang, *J. Phys. Chem. C.,* 2007, **111**, 4956-4963.

[43] C. Li, W. Guo, Y. Kong and H. Gao, *Appl. Phys. Lett.,* 2007, **90**, 223102.

[44] A. Jain, V. Kumar and Y. Kawazoe, *Comput. Mater. Sci.,* 2006, **36**, 258-262.

[45] R. Czerwieniec, J. Herbich, A.Kapturkiewicz and J. Nowacki, *Chem. Phys. Lett.,* 2000, **325**, 589-598.

[46] M.S. Gudipati, J. Daverkausen, M. Maus and G. Hohlneicher, *Chem. Phys.,* 1944, **186**, 289-301.

[47] S. Goswami, D. Sen, NK. Das, HK. Fun and CK. Quah, *Chem. Commun.,* 2011, **47**, 9101-9103.

[48] P. Goswami and D.K. Das, *J. Fluorsc.,* 2012, **22**, 391-395.